J. theor. Biol. (2001) **211,** 143–157
doi:10.1006/jtbi.2001.2336, available online at http://www.idealibrary.com on IDEAL®

Structural Changes in the Neck Linker of Kinesin Explain the Load Dependence of the Motor's Mechanical Cycle

A. MOGILNER*, A. J. FISHER† AND R. J. BASKIN†

*Department of Mathematics and Institute of Theoretical Dynamics, University of California at Davis, CA 95616, U.S.A. and †Section of Molecular and Cellular Biology, University of California at Davis, CA 95616, U.S.A.

(*Received on* 14 *April* 2000, *Accepted in revised form on* 19 *April* 2001)

The two-headed motor protein kinesin hydrolyzes ATP and moves on microtubule tracks towards the plus end. The motor develops speeds and forces of the order of hundreds of nanometers per second and piconewtons, respectively. Recently, the dependence of the velocity, the dissociation rate and the displacement variance on the load and the ATP concentration were measured *in vitro* for individual kinesin molecules (Coppin *et al*., 1997; Visscher *et al*., 1999) over a wide range of forces. The structural changes in the kinesin motor that drive motility were discovered by Rice *et al*. (1999). Here we present a phenomenological model for force generation in kinesin based on the bi-stable, nucleotide-dependent behavior of the neck linker. We demonstrate that the model explains the mechanical, kinetic and statistical (experimental) data of Coppin *et al*. (1997). We also discuss the relationship between the model results and experimental data of Visscher *et al*. (1999).

1. Introduction

Conventional kinesin is a motor protein that converts the energy of ATP hydrolysis into mechanical work, transporting organelles toward the plus end of microtubules (Bray, 1992). The motor is involved in intracellular transport, cell division and signal transduction (Goldstein & Philip, 1999). It serves as an important model system for understanding biological motility.

The motor 'walks' along a single microtubule (Ray *et al*., 1993) in a stepwise manner, using tubulin dimers as 'steps of the ladder'. It is not known whether this walk is performed along a single protofilament, or if the motor straddles two adjacent protofilaments. The length of a step is 8 nm (Svoboda *et al*., 1993), the same as the protofilament period. Kinesin mainly interacts with β-tubulin. This walk, at speeds of few hundreds of nanometers per second, is resisted by the viscous drag of the cytoplasm. At such speeds the viscous drag is negligible: the viscous drag on a sphere the size of kinesin moving at 1 μm/s is $\sim 10^{-4}$ pN. Even if the motor carries a cargo a few microns in size, the viscous drag is much less than 1 pN. However, at higher loads, the rate of motion slows down, and the motor is stalled by forces of 5–7 pN (Svoboda & Block, 1994; Visscher *et al*., 1999). The motor can therefore produce an energy of $\simeq 40$ pN nm per step, which is about 50% of the energy available from one ATP molecule (Bray, 1992).

Conventional kinesin is a highly processive motor able to move along more than 100 tubulin

*Author to whom correspondence should be addressed.

0022–5193/01/140143 + 16 $35.00/0

units before detaching (Block *et al.*, 1990; Vale *et al.*, 1996). An alternating site, enzymic mechanism of coupling the ATP hydrolysis cycle to a cycle involving conformational change in the protein has been proposed to explain such processive motion (Hackney, 1994; Gilbert *et al.*, 1998). Quantitatively, the essential features of kinesin's mechanical behavior were explained within a 'head-over-head' model (Peskin & Oster, 1995). In this model, asymmetry in the hydrolysis rate between the front and rear heads and the geometry of the head's binding and the associated power stroke drive the motor forward.

In the next section, we discuss the constraints that the existing experimental data impose on theoretical models. In Section 3, we introduce the model, and in Section 4, describe its mechanical cycle. The model is quantified in Section 5. The results of the mathematical analysis of the model are presented in Section 6. We conclude with a general discussion of kinesin models and their utility for biological problems in Section 7. The details of the computations are contained in the appendices.

2. Experimental Constraints on a Model

The structural, force-generating and enzymic properties of kinesin have been extensively studied. They place increasingly stringent constraints on theoretical modeling. Here we briefly describe the relevant experimental data that a model has to comply with.

2.1. STRUCTURAL DATA

Conventional kinesin is a heterotetrameric motor protein that contains two $\simeq 7$ nm globular domains—heads—connected to a $\simeq 75$ nm dimerized α-helical tail (Vale & Fletterick, 1997). The kinesin head has a ~ 330-amino acid catalytic core that binds ATP and microtubules. The nucleotide binding pocket is similar to that in myosin and G-proteins and contains similar switch regions. While kinesin is similar to other motors in its nucleotide binding pocket and some switch regions, it does not have a region similar to the myosin light chain stabilized α-helix. In the dimeric form of kinesin, the heads show a rotational symmetry of 120° about an axis close to that of the coiled coil. In this arrangement, the two heads could not have equivalent interactions with microtubules (Kozielski *et al.*, 1997).

Kinesin does not have an elongated lever arm to amplify small changes in the catalytic domain, like myosin, and has to rely on another type of mechanical element. The neck linker, a 15-amino acid segment, has proven to be important for kinesin's motility and directionality (Rice *et al.*, 1999).

Our model is based on the contention that the neck linker is able to dissociate from the catalytic core and function as both a tether and an elastic element (Fig. 1). Specifically, following (Rice *et al.*, 1999), we suggest that the kinesin β-10 sheet and the β-9 sheet, dissociate from the nucleotide-free or ADP-catalytic core. This dissociation creates, in effect, a tether which is about 5 nm long. This tether allows the diffusion of the free head along the substrate to the next binding site on β-tubulin. Strong binding of this head to the microtubule upon binding of ATP causes a 'zippering'—induced fit—of this portion of the kinesin heavy chain, which pulls it near the catalytic core. This movement functions as a power stroke and pulls the load along the microtubule.

2.2. MECHANICAL DATA

In the *in vitro* experiments, the motor tows a latex bead, which is joined to the hinge of the motor by an elastic tether. A load force, f, is applied to the bead by a laser trap. Originally, Svoboda & Block (1994), and more recently, Coppin *et al.* (1997) and Visscher *et al.* (1999) used a laser-trap-based system to investigate the mechanical behavior of kinesin.

Coppin *et al.* (1997) measured the load dependence of the motor's average velocity. They discovered that the speed is almost insensitive to loads of magnitude less than $\simeq 2$ pN. At backward loads of greater magnitude, which resist the motor's forward walk, the velocity decreased in an almost linear fashion to a stall force of $\simeq 5$–6 pN. Under a forward load of $\simeq 2$–6 pN, the velocity increased significantly, two- to threefold, compared to free movement. Coppin *et al.* (1997) also observed that kinesin does not walk backwards at backward loads greater than the stall load.

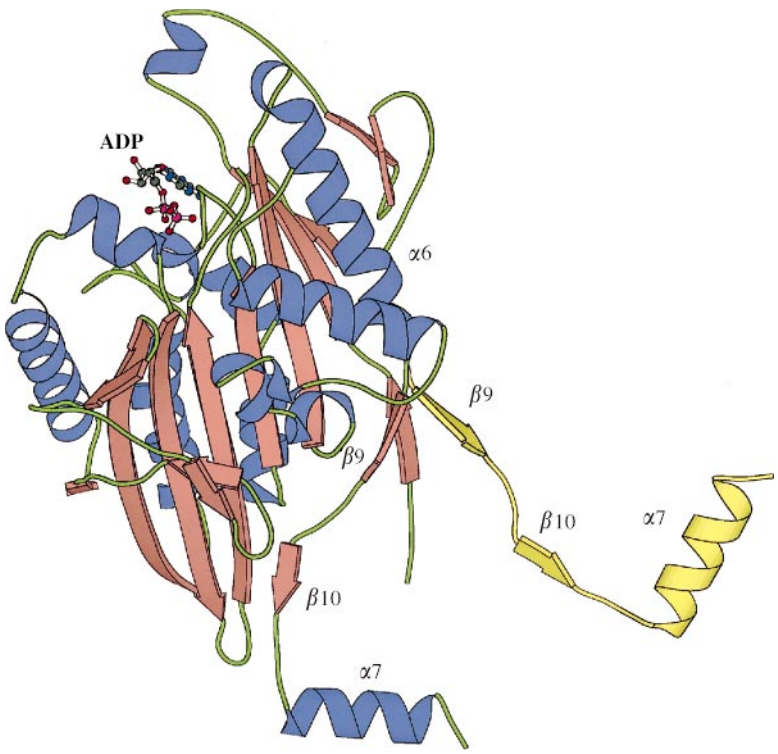

FIG. 1. Crystal structure of kinesin motor and neck domain (PDB accession number: 2KIN, Sack *et al*., 1997) displayed in a Richardson ribbon cartoon. The α-helices and β-strands are displayed as blue coils and red arrows, respectively. Shown in yellow is the carboxyl terminal neck linker domain (β-9, β-10 and α-7) as possibly oriented in the backward pointing state in the model. The bound ADP molecule is displayed as ball-and-stick to identify the active site. The figure was generated with the program MOLSCRIPT (Kraulis, 1991).

Further, the dissociation rate of the motor from the fiber increased as a function of backward load up to a spontaneous stall (5–6 pN), and then became insensitive to load at the induced stall force (for forces up to 12 pN).

In this paper, we explain quantitatively the load dependent behavior of kinesin observed by Coppin *et al.* (1997). In Section 6.4, we discuss the relationship of our model to the results of Visscher *et al.* (1999).

2.3. KINETIC DATA

Kinesin hydrolyzes one ATP molecule for each 8-nm step (Coy *et al.*, 1999). The motor's average velocity increases almost linearly with ATP concentration (at small concentrations in the μM range). At larger ATP concentrations the growth slows down and saturates at high concentrations in the mM range (Coppin *et al.*, 1997; Visscher *et al.*, 1999).

The motor's displacement variance increases linearly with time. The rate of this increase, over a wide range of ATP concentrations and at low loads, is close to a half of the rate of a corresponding Poisson stepper with an 8 nm step size (Svoboda *et al.*, 1994; Visscher *et al.*, 1999). At a high backward load, this rate increases to almost the rate of a corresponding Poisson stepper (Visscher *et al.*, 1999). Our model explains this behavior.

3. Description of the Model

We assume that only one head of the motor can bind to each β-tubulin site at a given time. These sites are located at a distance $\delta = 8$ nm apart. The two heads of the motor are connected at a hinge, to which the load force f is applied. Note that in the experiments of Coppin *et al.* (1997) and Visscher *et al.* (1999) the force was applied to a micron-sized bead connected to the kinesin molecule through an elastic tether, not directly as assumed in the model. We discuss this assumption in Appendix A. The force is measured in the direction of the minus end of a microtubule, so that positive and negative values of force correspond to backward and forward loads, respectively.

In the model, each head of a kinesin molecule has two possible tubulin affinity states, high and low. In the low affinity state, the head diffuses along the microtubule and does not bind to an empty β-tubulin site. In the high affinity state, the head is firmly bound to a β-tubulin site.

Following Rice *et al.* (1999), we assume that the behavior of the neck linker of a kinesin motor head is nucleotide dependent. When an ATP or an ADP-P_i molecule is bound to the head, the neck linker is docked to the motor head's catalytic core in the forward-pointing state. On the other hand, when an ADP molecule is bound to the head, or the head is nucleotide free, the neck linker fluctuates rapidly between the backward- and forward-pointing states (the ADP-forward state is different from the docked ATP-state). The ATP and ADP-P_i-heads are in the high affinity state (strongly bound), while the ADP and nucleotide-free heads are weakly bound to the microtubule.

The bias for plus-end directed motion is generated through (i) the asymmetry of a head binding to a β-tubulin state and the accompanying neck linker docking; (ii) the highly coordinated nucleotide hydrolysis in the forward and backward pointing heads; and (iii) the asymmetry of ATP binding. When an ATP molecule is bound to one of the heads, its neck linker–forward-pointing docking causes the other head to bind closer to the microtubule plus end. The ATP/ADP exchange in the rear head and the ADP/ATP exchange in the front head (corresponding to a sequence of transitions as described in the next section) trigger the dissociation of the rear head. Rezippering of the neck linker in the front head displaces the rear head by 16 nm to the next β-tubulin site. The net result of this action is an 8 nm step of the kinesin molecule.

Both a Brownian ratchet, and a power stroke produce a step and generate force in the model. First, ATP binding rectifies thermal fluctuations of the neck linker between the two states. Second, it induces elastic strain in the backward-pointing state of the neck linker. Third, it rectifies the 'zippering' Brownian ratchet of the neck linker when it is in the forward-pointing state. Finally, it may change the neck coiled-coil interactions that could augment the plus-end bias.

Using a mathematical model, we will demonstrate that a backward load slows down the motor by biasing the neck linker to the backward-pointing state, and decreasing the rate

of the neck linker docking. A forward load speeds up movement by biasing the neck linker to the forward-pointing state.

4. The Mechanical Cycle

Figure 2a shows the essential features of the motor cycle. We begin from the state z_j, in which both heads are bound to adjacent sites, 8 nm apart (j is the index of tubulin dimers along a microtubule protofilament). ATP is bound to the rear head, and the docked neck linker keeps the front ADP–motor head complex bound to the microtubule. The hydrolysis and release of the phosphate group from the rear head and the release of ADP from the front head occur with an effective rate of k_1. In the model, this rate is independent of the ATP concentration. Note that here we 'bundle together' several chemical transitions to simplify the illustration of kinetic partitioning and the resulting processivity of the motor. The validity of this approach will be determined by future work. In the next state u_j, the nucleotide-free head remains bound to the microtubule, while the other head executes (rapid) thermal motion between the backward and the forward positions corresponding to the respective conformations of the neck linker. ATP binds to the microtubule bound head of kinesin, with rates k_2 and k_3 in the forward- and the backward-pointing states of the neck linker, respectively. If the binding occurs in the forward state, we assume that the neck linker 'zippering' takes place rapidly. It is also load independent because of the very small distance along the microtubule between the forward pointing nucleotide-free state and the ATP-bound state. Thus, when the ATP binding takes place in the forward pointing state, the motor goes into the state z_{j+1}, which completes the cycle. When the ATP binding takes place in the backward pointing state, we assume that the neck linker initially becomes strained, and then swings forward and 'zippers' with an effective load-dependent rate k_4. This is a second pathway for completing the cycle. The key parameters of this model are presented in Table 1.

Note that in the model, one ATP is hydrolyzed during each cycle. Although the mechanical cycle does not uniquely determine the kinetic parameters, the mechanical cycle in the model is similar to the kinetic scheme proposed by Gilbert *et al.* (1998) (the ADP release step is different). Also note that all chemical steps in the model are taken to be irreversible. In fact, we assume that all backward transitions in the suggested mechanical cycle are characterized by rates, which are very slow in comparison with the corresponding forward rates. Therefore, the respective transitions can be neglected in calculations of the average kinetic and mechanical characteristics of the motor. This assumption can be justified, for the transition from the zippered to the unzippered state, by the fact that this transition is associated with the release of the phosphate group. The experiments are performed at low concentrations of the hydrolysis products, so the corresponding backward rate is very small. Our omission of transitions from the zippered to the strained state is based on the assumption that zippering is associated with a large decrease in free energy (in comparison with thermal energy). ATP binding is known to be reversible. However, our numerical analysis demonstrated that the corresponding backward rate does not (in a qualitative way) affect the theoretical results.

It was suggested by Coppin *et al.* (1997) that the results on the load dependence of the kinesin dissociation rate can be explained by a load dependent partitioning between two kinetic pathways. We will demonstrate here that this is indeed the case.

5. The Mathematical Model of the Force Generating Cycle

At the instant of the transition from the zippered to the unzippered state of the neck linker, the free kinesin head begins to fluctuate between the backward and the forward pointing states, Rice *et al.* (1999) observed that the backward and forward positions are similar in energy, and that transitions between these states are very rapid. These observations were made on monomeric kinesin. We will assume that in the backward position, the effective interaction of the free head with the microtubule lowers the corresponding energy of the backward state by a few k_BT. We will also assume that the maximum position of an effective energy barrier between the two states is

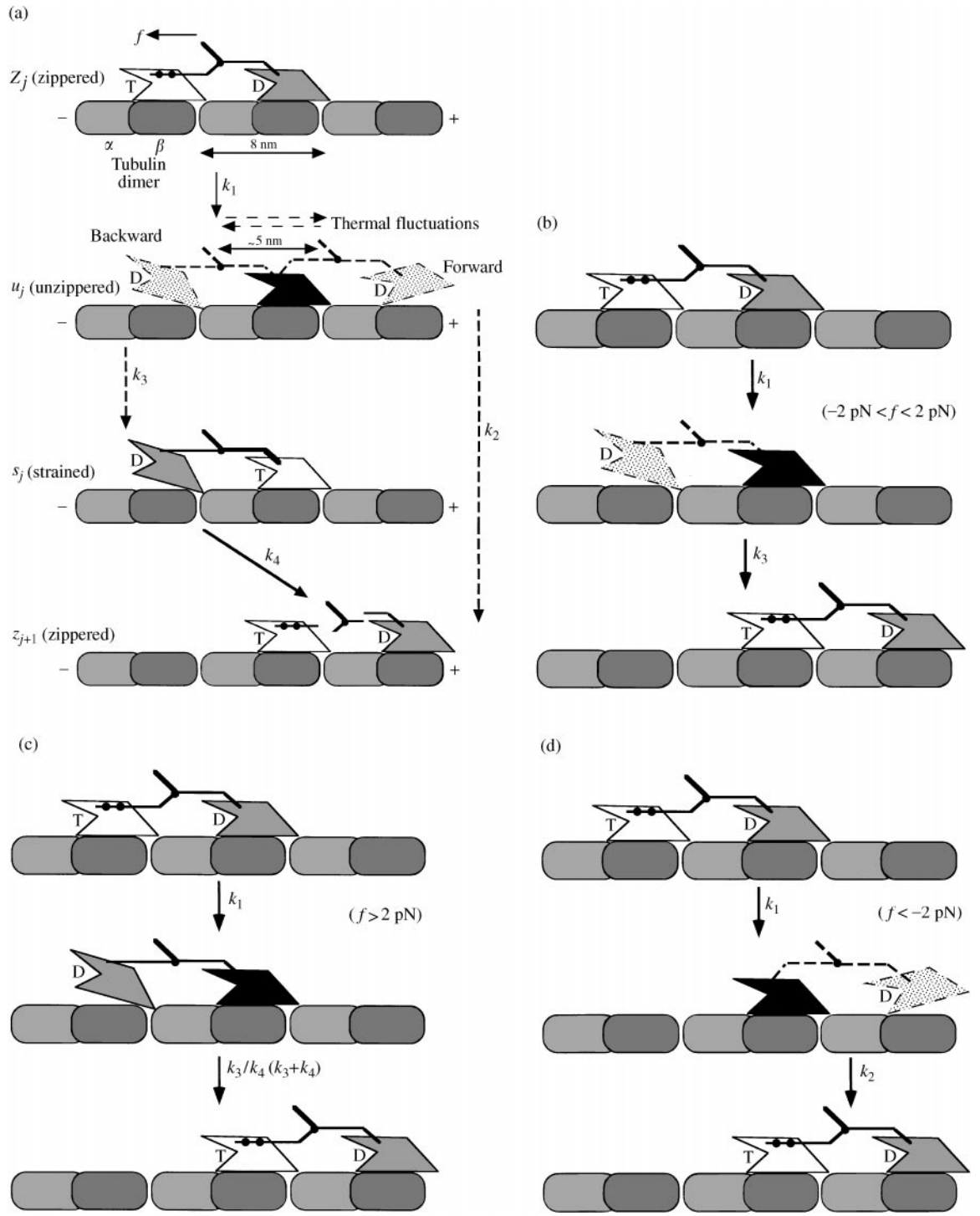

FIG. 2. (a). Essentials of the mechanical motor cycle. Different shading of kinesin heads indicates different conformations that depend on both binding (strong and weak) and chemical states. T and D stand for ATD and ADP respectively. Empty 'pocket' corresponds to the nucleotide-free state. Dashed arrows indicate the alternative pathways. Other details are in the text. (b). Simplified two-step mechanical cycle in the case of moderate loads. (c). Simplified two-step mechanical cycle in the case of large backward loads. (d). Simplified two-step mechanical cycle in the case of large forward loads.

located close to the backward pointing state, such that the load does not significantly affect the transition time between the states.

The diffusion time, $\tau \sim 10^{-5}$–10^{-3} s, of the kinesin head over distances on the order of 16 nm is brief in comparison with the mean life times of

TABLE 1
Model parameters

Symbol	Value	Meaning
k_BT	4.1 pN nm	Thermal energy
δ	8 nm	Kinesin step size = distance between β-tubulin sites along microtubule protofilament
f	From -6 pN to 6 pN	Load force
W	$5\,k_BT$	Free energy difference between the forward and backward pointing state of the neck linker
L	5 nm	Separation between the forward and backward pointing state of the neck linker
k_1	$50\ s^{-1}$	Rate of hydrolysis/unbinding of the back head
k_2	$120\ s^{-1}$ at 1 mM ATP, $80\ s^{-1}$ at 40 μM ATP, $15\ s^{-1}$ at 5 μM ATP	Rate of ATP binding in the backward pointing state of the neck linker
k_3	$35\ s^{-1}$ at 1 mM ATP, $25\ s^{-1}$ at 40 μM ATP, $5\ s^{-1}$ at 5 μM ATP	Rate of ATP binding in the backward pointing state of the neck linker
$k_4(0)$	$2.5\times10^3\ s^{-1}$	Rate of the zippering of the neck linker at zero load
k_u	$0.12\ s^{-1}$	Dissociation rate from the conformation with the backward pointing state of the neck linker and no ATP bound
k_s	$2\ s^{-1}$	Dissociation rate from the conformation with the backward pointing state of the neck linker and ATP bound

the different states of the cycle, $\sim 10^{-2}$ s. (For the free diffusion, $\tau \sim (16\text{ nm})^2/(10^7\text{ nm}^2/\text{s}) \sim 10^{-5}$ s, where 10^7 nm^2/s is the order of magnitude of the diffusion coefficient of the kinesin head. It is brief even when multiplied by the Arrhenius factor, $\exp(5k_BT/k_BT) \sim 100$, where $5k_BT$ is the likely height of the energy barrier between the states.) Thus, we can average over the different head positions that are in thermodynamic equilibrium. From the Boltzmann distribution, we find that the ratio of the expected occupancies of the forward- and backward-pointing states is $\exp((-W-Lf)/k_BT)$. Here W is the free energy difference between the states of the neck linker, $L \simeq 5$ nm is the separation between the forward- and backward-pointing states (Rice *et al.*, 1999), and f is the load force. Neglecting the time spent by the head in its transition between the two states, we obtain the load-dependent probability for the free head to be in the forward state:

$$p(f) = \frac{\exp((-W-Lf)/k_BT)}{1+\exp((-W-Lf)/k_BT)}, \qquad (1)$$

while the probability for the head to be in the backward state is $(1-p(f))$.

The rate of transition from the strained state of the neck linker to the zippered position, $k_4(f)$, is assumed to be load dependent, because this transition implies a forward movement comparable to L. According to the analysis of Fisher & Kolomeisky (1999), the effect of the load may be taken into account by modifying the forward and backward transition rates ($k_4(0)$ and $k_{-4}(0)$, respectively) according to $k_4(f) = k_4(0)\exp(-\theta_+ Lf/k_BT)$ and $k_{-4}(f) = k_{-4}(0)\exp(\theta_- Lf/k_BT)$. Here θ_+ and θ_- are load distribution factors which reflect how the external force affects the individual rates, $\theta_+ + \theta_- = 1$. As we discussed above, we assume that the (individual) backward rate $k_{-4}(0)$ is negligibly small. Furthermore, we will assume that $\theta_+ \simeq 1 \gg \theta_-$, so that:

$$k_4(f) \simeq k_4(0)\exp(-Lf/k_BT). \qquad (2)$$

A similar assumption is usually made in simple models of a polymerization ratchet (Peskin *et al.*, 1993).

The separation of time scales between the faster molecular diffusion rate and the slower transition rate between chemical states reduces the motion of the motor to a Markov chain

governed by the following system of equations [see Fig. 2(a)]:

$$\frac{dz_j}{dt} = -k_1 z_j + \tilde{k}_2 u_{j-1} + \tilde{k}_4 s_{j-1},$$

$$\frac{du_j}{dt} = k_1 z_j - (\tilde{k}_2 + \tilde{k}_3) u_j,$$

$$\frac{ds_j}{dt} = \tilde{k}_3 u_j - \tilde{k}_4 s_j, \qquad (3)$$

$$\tilde{k}_2 = k_2 p(f), \quad \tilde{k}_3 = k_3(1 - p(f)), \quad \tilde{k}_4 = k_4(f).$$

6. Results

6.1. THE LOAD-VELOCITY RELATION

The eqn (3) are solved analytically in Appendix B to obtain the following dependence of the average rate of the motor's motion on the load:

$$\langle v \rangle = \delta \left[\frac{1}{k_1} + \frac{1}{\tilde{k}_2 + \tilde{k}_3} + \frac{\tilde{k}_3}{\tilde{k}_4(\tilde{k}_2 + \tilde{k}_3)} \right]^{-1}. \qquad (4)$$

We can choose the parameter values of W, k_1, k_2, k_3, $k_4(0)$ to fit the experimental data of Coppin *et al.* (1997) (see Table 1). We then choose the values of W, k_1, $k_4(0)$ such that they are ATP independent. The rates of ATP binding k_2, k_3 increase with increasing ATP concentration to saturation (according to Michalis–Menten kinetics). We set the ratio k_2/k_3 to be ATP independent. All the rates and characteristic distances are of the same order of magnitude as those known from the experimental values. The value (and even the sign) of the free energy parameter W is unknown. The assumption that the backward-pointing state has a lower energy, than that of the forward-pointing state, is crucial to our model. If the magnitude of parameter W is greater than $5k_BT$, then the fit to the experimental data will be even better. However, if W is less than $5k_BT$, the 'plateau' region in the force–velocity curve becomes less pronounced.

The theoretical force–velocity relation (4) shows a good fit to the experimental data (Fig. 3). Here it is clearly seen that there are three distinctive load-dependent regimes of kinesin movement.

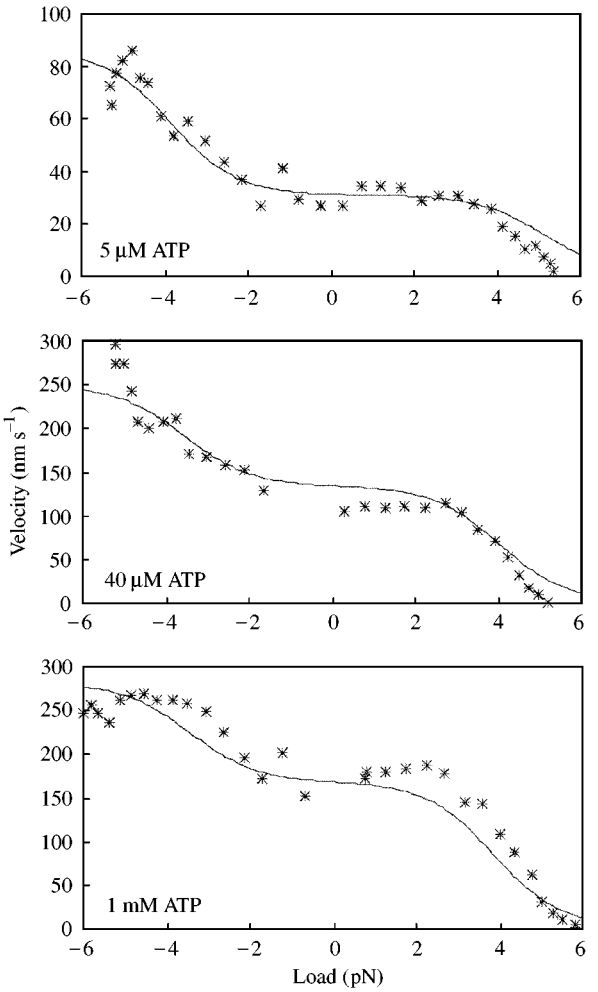

FIG. 3. Force-velocity relations for three different ATP concentrations. The theoretical relations predicted by eqn (4) are plotted with the solid lines. The stars represent the experimental results of Coppin *et al.* (1997).

(1) Moderate loads; nearly free motion (-2 pN $< f < 2$ pN).

At a small load force, the load dependence of the occupancies of the forward- and backward-pointing states of the neck linker are negligible. The neck linker is in the backward-pointing state most of the time. When ATP binds, the transition of the strained neck linker into the zippered state occurs with rate $k_4(0)\exp(-Lf) > 200\,s^{-1} \gg k_3$. The mechanical cycle simplified into a detachment of the rear head with the load-independent rate k_1, and its subsequent attachment with the load-independent rate k_3 [Fig. 2(b)]. The corresponding load-independent velocity is the step

length divided by the duration of the cycle:

$$\langle v\rangle \simeq \delta \frac{k_1 k_3}{k_1 + k_3}.$$

(2) High backward loads; nearly stalled motion ($f > 2$ pN).

At a larger positive (backward) force, the cycle still goes through the pathway associated with the backward state of the neck linker [Fig. 2(c)]. However, at a large load, the load-dependent rate of zippering, $k_4(f)$ becomes comparable with the rate of ATP binding, and an effective rate of head attachment can be computed as $(k_4 k_3/(k_4 + k_3))$. At very great loads, $f > 5$ pN, $k_4(f) \ll k_3$, and $(k_4 k_3/(k_4 + k_3)) \simeq k_4$. The duration of the cycle because $k_1^{-1} + k_4^{-1} \simeq k_4^{-1}$ (at $f > 5$ pN, $k_4(f) \ll k_1$), so that the average rate of the nearly stalled motion is:

$$\langle v\rangle \simeq \delta k_4(f) = \delta k_4(0)\exp(-Lf).$$

Thus, the velocity decreases exponentially with force at large backward loads in an ATP-independent way. There is no possibility of backward motion in our model. The model predicts that at a backward load of the order of 6 pN, the rate of motion becomes so small that the dissociation of the kinesin molecule from the mictrotubule occurs within one cycle. We discuss the relationship of our results to the observations of Visscher *et al.* (1999) in Section 6.4.

(3) High forward loads; accelerated motion ($f < -2$ pN).

At a large negative (forward) force, the probability of the forward pointing state of the neck linker becomes greater than that of the backward state [Fig. 2(d)]. The simplified, attachment–detachment mechanical cycle, goes through an alternative pathway. This leads to an acceleration of the head movement because the rate of ATP binding in the forward state is assumed to be greater, and the rate of zippering from the forward state is load independent. The effective rate of attachment at great forward loads, $f < -5$ pN, becomes k_2, the duration of the cycle $k_1^{-1} + k_2^{-1}$, and the rate of motion:

$$\langle v\rangle \simeq \delta \frac{k_1 k_2}{k_1 + k_2}.$$

The motor accelerates $(k_2(k_1 + k_3)/k_3(k_1 + k_2))$ times in comparison with the zero load case (1.7 times at 1 mM of ATP, 1.8 times of 40 μM of ATP, 2.5 times at 5 μM of ATP).

6.2. LOAD-DEPENDENT DISSOCIATION KINETICS

The processivity of the kinesin molecule is high; it moves along a microtubule for as many as ~100 steps. In our model, we assume that the rate of dissociation of the motor from the microtubule is negligible when the motor–neck linker is in the zippered state and both heads are bound. The dissociation rate of the motor from the unzippered state, k_u, is relatively low, while that from the strained state, k_s, is high. We also assume these rates to be load independent. In Appendix B we compute the resulting net dissociation rate γ:

$$\gamma(f) = \frac{k_u \tilde{k}_4 + k_s \tilde{k}_3}{\tilde{k}_4 + (\tilde{k}_2 \tilde{k}_4/k_1) + \tilde{k}_3(1 + (\tilde{k}_4/k_1))}. \quad (5)$$

We plot its load dependence in Fig. 4. The parameter value k_u was chosen to give the known processivity at zero load. The value of k_s was chosen to fit the experimental results of Coppin *et al.* (1997) (see Table 1). Our explanation for the observed behavior of the dissociation rate is that at low loads the motor is almost never in the strained state because the transition to the zippered state is very fast. As a result, the processivity is high. At high loads, $f > 5$ pN, the stalled motor is almost always in the strained state, from which the zippering is very slow. The dissociation rate becomes high and load independent above a value of 5 pN.

6.3. LOAD DEPENDENCE OF FLUCTUATIONS IN DISPLACEMENT

If the motor is progressing by random Poisson steps of length δ, at a rate δ/T, then the variance in its position will grow linearly with time at the rate δ^2/T (Van Kampen, 1981). In other words, if the average rate of motion of the 'Poisson stepper' is $\langle v\rangle$, then the rate of growth of the variance in its position would be $\delta\langle v\rangle$. The actual rate is considerably less than this. This indicates that more than one rate limiting step is involved in each cycle of the motor.

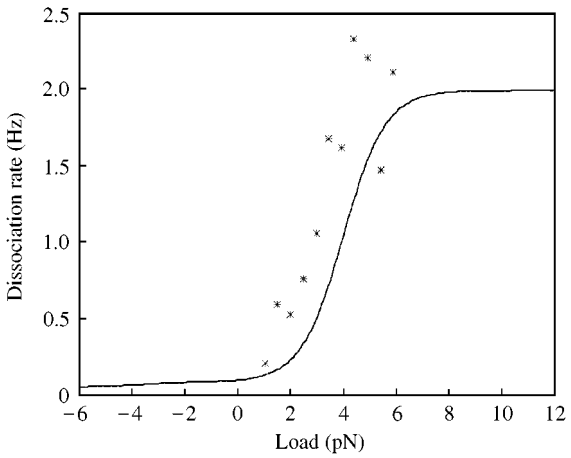

FIG. 4. Load dependence of the dissociation rate given by eqn (5) is shown by the solid line. The stars represent the experimental results of Coppin *et al.* (1997).

In Appendix B we compute the so-called randomness parameter, r, (Svoboda *et al.*, 1994) showing the ratio of the actual rate of growth of the displacement variance to that of a 'Poisson stepper' moving with the same speed:

$$r = 1 + 2\,\frac{k_1^2\tilde{k}_2\tilde{k}_3 - k_1\tilde{k}_2\tilde{k}_3\tilde{k}_4 - k_1^2\tilde{k}_3\tilde{k}_4 - k_1\tilde{k}_3^2\tilde{k}_4 - k_1\tilde{k}_2\tilde{k}_4^2 - k_1\tilde{k}_3\tilde{k}_4^2}{(k_1\tilde{k}_4 + k_1\tilde{k}_3 + \tilde{k}_4(\tilde{k}_2 + \tilde{k}_3))^2}. \tag{6}$$

The load dependence of the randomness parameter at different ATP concentrations is shown in Fig. 5. For moderate loads, $-2\,\text{pN} < f < 2\,\text{pN}$, the randomness parameter is load independent. It is close to 0.55 at moderate and high ATP concentrations and it is about 0.85 at 5 μM ATP.

At significant backward loads, of about 3 pN (at moderate and high ATP concentrations), and loads of 5 pN at 5 μM ATP, the randomness parameter decreases to 0.35. This supports the notion that at these loads and ATP concentrations the cycle of kinesin consists, in effect, of three transitions of similar duration. (The randomness parameter of a stepper motor, each step of which is accomplished after three random transitions with equal transition rates, is equal to 1/3.) At high backward loads, the randomness parameter increases rapidly for all ATP concentrations approaching the value of 1, almost that of a Poisson stepper motor.

At significant forward loads, r does not change significantly for moderate and high ATP concentrations: it stays between 0.5 and 0.6. At low ATP concentrations, the randomness parameter significantly decreases at forward loads. Coppin *et al.* (1997) did not measure the load dependence of the variance of the motor's displacement. We will discuss the relationship of our results to the experimental data of Visscher *et al.* (1999) in the next section.

6.4. THE RELATIONSHIP BETWEEN THE MODELING RESULTS AND THE DATA OF VISSCHER *ET AL.* (1999)

There are significant differences in the experimental results of Coppin *et al.* (1997) and those of Visscher *et al.* (1999). These differences may stem from the fact that the kinesin molecules studied were moving on sea urchin axonemes in the former experiments, and on microtubules in the latter experiments. Also, Visscher *et al.* (1999) used methods of measuring force and displacement that were of a higher resolution than Coppin *et al.* (1997). It is not possible to explain, quantitatively, the difference between the experimental results within the framework of our model, using a single set of parameters, because binding to the track (axonemes or microtubules) is coupled to a particular transition between states of the kinesin cycle.

Here we discuss changes in our model that could explain the data of Visscher *et al.* (1999).

6.4.1. *Randomness parameter*

Visscher *et al.* (1999) observed that at a 2 mM ATP concentration, the randomness parameter has values between 0.35 and 0.5 for loads between 0 and 5 pN. This parameter increases to 1.2 when the load increased from 5 to 6 pN. These data agree qualitatively with the results of our model at high ATP concentration [1 mM; see our Fig. 5 and Fig. 4(b) of Visscher *et al.* (1999)]. The fact that our model does not allow for the

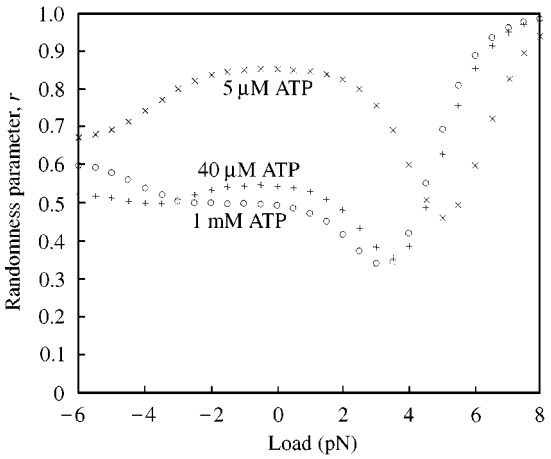

FIG. 5. Theoretically predicted load dependence of the randomness parameter at three different ATP concentrations given by eqn (6).

randomness parameter to be greater than 1, is due to our assumption that all the backward transition rates are negligibly small. This assumption is likely to become inadequate at either high loads, or small ATP concentrations, when some forward transitions are slowed down.

Our results show that at low backward loads, the randomness parameter decreases as the ATP concentration increases. However, at high backward loads, the randomness parameter increases slightly as the ATP concentration increases. Qualitatively, these predictions agree with the measurements of Visscher *et al.* (1999) [see their Fig. 4(a)]. As we noted above, a different set of transition rates is necessary in order to precisely fit their experimental data.

6.4.2. *Load-velocity relation*

The most remarkable experimental result of Visscher *et al.* (1999) was that the 'stall force' depends on ATP concentration: it increases from ~ 5.5 pN at ATP concentrations in the μM range to ~ 7 pN at ATP concentrations in the mM range. Also, at small backward loads, the load–velocity curve showed a steeper slope than that of Coppin *et al.* (1997). This slope also depended on ATP concentration: the velocity decreased faster with the growth of the load at lower concentrations of ATP [Fig. 3(a) of Visscher *et al.* (1999)]. Let us note that the observed 'stall force' is not the force at which the kinesin advancement stops completely: both our model, and that of Schnitzer *et al.* (1999) predict exponental decrease of the velocity to zero at high loads. The 'stall force' is defined, effectively, by the extrapolation of the force–velocity curve from high (4–6 pN) loads to very high (>6 pN) loads.

In the framework of our model, one possible explanation for the dependence of the stall force on ATP concentration is based on the assumption that the catalytic core of the motor is modified at high backward loads, when bound to a microtubule. Namely, a load-induced strain effectively decreases the rate of ATP binding. Quantitatively, we can assume that the corresponding rate constant k_3 (of ATP binding in the backward pointing state) is changed by the load-dependent factor $(p_c + (1 - p_c)\exp(fl/k_BT))^{-1}$. This assumption is valid when the corresponding step consists of a load-independent biochemical transition followed by a load-dependent mechanical transition (Schnitzer *et al.*, 1999). The parameter p_c is the fraction of time required for the unloaded biochemical transition, and l is the length of the effective step associated with the mechanical transition. For the model to be consistent, we have to reduce the effective distance associated with the transition from the strained state of the neck linker to the zippered position: the load dependence of the rate $k_4(f) = k_4(0)\exp(-fL/k_BT)$ has to be changed to $k_4(f) = k_4(0)\exp(f(l - L)/k_BT)$. We introduced these changes into eqn (4) and used the parameters $l = 2.5$ nm and $p_c = 0.9$ at 5 μM ATP and $p_c = 0.8$ at a 1 mM ATP concentration to obtain the modified force–velocity curves shown in Fig. 6. These curves are in good qualitative agreement with the results of Visscher *et al.* (1999) [see their Fig. 3(a)].

6.4.3. *Dissociation kinetics*

Schnitzer *et al.* (2000) both showed experimentally, and modeled theoretically the load dependence of kinesin processivity. They observed that the mean run length increased with an increase in the ATP concentration to saturation and exhibited Michaelis–Menten behavior. The mean run length increased significantly as the ATP concentration grew at low loads, and less

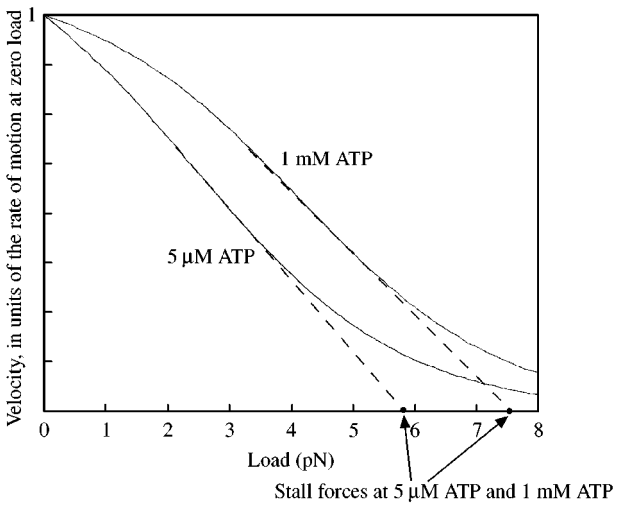

FIG. 6. The modified force–velocity curves at high and low ATP concentrations show that the stall force is an increasing function of ATP concentration. The curves are obtained by modifying the model as described in Section 6.4.

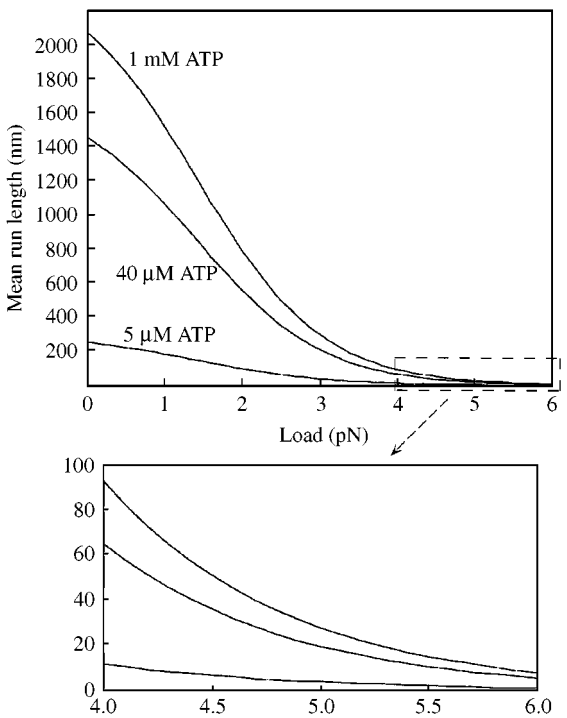

FIG. 7. The mean run length is defined as $\langle v \rangle / \gamma$ and is computed using formulae (4) and (5) as a function of the load at three different ATP concentrations. Shown below is an expanded plot of the data at high loads.

significantly at high loads. In keeping with our model, the model of Schnitzer *et al.* (2000) was based on the dissociation of kinesin involving two states in the mechanochemical cycle.

The mean run length can be defined as the average velocity times the average time before dissociation, or as the average velocity divided by the effective dissociation rate, $\langle v \rangle / \gamma$. We used formulae (4) and (5) to compute the dependence of the mean run length on the load and ATP concentration. The results shown in Fig. 7 are in qualitative agreement with the corresponding data of Schnitzer *et al.* (2000).

7. Conclusions, Predictions and Discussion

Our model quantifies the mechanical cycle of the kinesin molecule suggested by Rice *et al.* (1999). It is based on nucleotide-dependent conformation transitions of the neck linker. In our model, as in that of Peskin & Oster (1995), part of each step is accomplished due to elastic deformation; a similar distance is covered due to thermal diffusion. Our mathematical model accounts for the experimental data of Coppin *et al.* (1997) on the load dependence of the velocity and the dissociation rate. We were able to explain the acceleration of the motor at high forward loads and the load-independent regime of the motor at moderate loads. Our conclusions confirm the predictions of Coppin *et al.* (1997) and Rice *et al.* (1999) concerning the existence of two alternative pathways of the kinesin cycle that are coupled to two conformations of the neck linker region of the molecules.

We base our model on a strong coordination between the hydrolysis cycle in each of the two motor heads, similar to (Peskin & Oster, 1995). One of the main differences between our model and that of Peskin & Oster is that we used a different mapping of the mechanical cycle onto the mechanochemical cycle in order to conform fully to the qualitative ideas of Rice *et al.* (1999). However, this is not of primary importance for understanding the mechanical behavior of kinesin. More importantly, Peskin & Oster (1995) assumed free diffusion of the free head (information about the two states of the neck linker was not available) and explained the 'plateau' in the force–velocity curve at moderate loads as due to subtle effects in the interaction of the neck with the elastic tether. In our model, this plateau is explained by the load-independent pathway of the kinesin walk at small loads, due to an energy

difference between the two states of the neck linker.

Two quantitative predictions of our model that can be used to test its adequacy are:

(1) According to our calculations of the load dependence of the dissociation rate, the processivity of the motor will almost double at high forward loads. Not only will the motor move faster, it also will travel a greater distance before dissociation.

(2) At forward loads and low ATP concentrations (of the order of a few μM), the randomness of the motor's motion should decrease significantly.

Schnitzer *et al.* (2000) and Fisher & Kolomeisky (2001) employed multi-state chemical kinetic models to explain quantitatively the data of Visscher *et al.* (1999). The model of Schnitzer *et al.* (2000) is based on the assumption of the existence of a load-dependent, conformationally composite state in the kinesin cycle. In this model, there are two effects of the load on catalysis of ATP occuring immediately after ATP binding. The model successfully fits the data of Visscher *et al.* (1999) relating the ATP concentration and the load dependence to the average velocity of the motor. The theory also fits the data of Schnitzer *et al.* (2000) on the relationship between the ATP concentration and the load dependence of the dissociation kinetics of the motor. The experimental results of Visscher *et al.* (1999) on the ATP concentration and the load dependence of the randomness parameter, as well as the results of Coppin *et al.* (1997) at forward loads were not modeled by Schnitzer *et al.* (2000). The model of Fisher & Kolomeisky (2001) is of a purely kinetic character. It is extremely successful in fitting the model results with virtually all known quantitative experimental data. Notably, this model predicts acceleration of kinesin at forward loads. However, the characteristic 'plateau' in the load–velocity curve at small loads is not predicted by this model.

Our modeling philosophy is the following. We believe that a theoretical model should explain some of the currently available experimental data in detail, and some of the data qualitatively. Then, despite existing controversy between different theories and experimental results, successive models will evolve into an adequate picture. Earlier theoretical models of kinesin, most notably those of Duke & Leibler (1996) and Derenyi & Vicsek (1996), were very valuable for the development of the current theories.

Finally, let us note that however informative and non-trivial kinetic models are, it is clear that complex combinations of the ratchet action and the power stroke can fit most any data (Keller & Bustamante, 2000). Nevertheless, such models are a necessary first phenomenological step towards a complete molecular model. The ultimate future goal will be to model, in molecular detail, the pathway of the energy transfer between the motor's catalytic site, the tubulin binding site, and the motors neck linker region.

We would like to thank G. Oster, R. Vale and A. Kolomeisky for valuable discussions. AM was supported by NSF Grant DMS 0073828 and NSF RTG Grant DBI-9602226. A portion of this work was performed under the auspices of the US Department of Energy by the University of California Lawrence Livermore National Laboratory, through the Institute for Laser Science and Applications, under contract No. W-7405-Eng-4 (LS01-004 to RJB).

REFERENCES

BLOCK, S. M., GOLDSTEIN, L. S. & SCHNAPP, B. J. (1990). Bead movement by single kinesin molecule with optical tweezers. *Nature* **348,** 348–352.

BRAY, D. (1992). Cell Movements. New York: Garland.

COPPIN, C. M., PIERCE, D. W., HSU, L. & VALE, R. D. (1997). The load dependence of kinesin's mechanical cycle. *Proc. Natl Acad. Sci. U.S.A.* **94,** 8539–8544.

COY, D. L., WAGENBACH, M. & HOWARD, J. (1999). Kinesin takes one 8-nm step for each ATP that it hydrolyzes. *J. Biol. Chem.* **274,** 3667–3671.

DERENYI, M. & VICSEK, F. (1996). The kinesin walk: a dynamic model with elastically coupled heads. *Proc. Natl Acad. Sci. U.S.A.* **93,** 6775–6779.

DUKE, T. & LEIBLER, S. (1996). Motor protein mechanics: a stochastic model with minimal mechanochemical coupling. *Biophys. J.* **71,** 1235–1247.

ELSTON, T. (2000). A macroscopic description of biomolecular transport. *J. Math. Biol.* **41,** 189–206.

FISHER, M. & KOLOMEISKY, A. (1999). The force exerted by a molecular motor. *Proc. Natl Acad. Sci. U.S.A.* **96,** 6597–6602.

FISHER, M. & KOLOMEISKY, A. (2001). Simple mechanochemistry describes the dynamics of kinesin molecules. *Proc. Natl Acad. Sci. U.S.A.*, In press.

GILBERT, S. P., MOYER, M. L. & JOHNSON, K. A. (1998). Alternating site mechanism of the kinesin ATPase. *Biochemistry* **37,** 792–799.

GOLDSTEIN, L. S. B. & PHILIP, A. V. (1999). The road less traveled: emerging principles of kinesin motor utilization. *Annu. Rev. Cell. Dev. Biol.* **15,** 141–183.

HACKNEY, D. D. (1994). Evidence for alternating head catalysis by kinesin during microtubule-stimulated

ATP hydrolysis. *Proc. Natl Acad. Sci. U.S.A.* **91,** 6865–6869.
KELLER, D. & BUSTAMANTE, C. (2000). The mechanochemistry of molecular motors. *Biophys. J.* **78,** 541–556.
KOZIELSKI, F., SACK, S., MARX, A., THORMAHLEN, M., SCHONBRUNN, E., BIOU, V., THOMPSON, A., MANDELKOW, E.-M. & MANDELKOV, E. (1997). The crystal structure of dimeric kinesin and implications for microtubule-dependent motility. *Cell* **91,** 985–994.
KRAULIS, P. J. (1991). MOLSCRIPT: a program to produce both detailed and schematic plots of protein structures. *J. Appl. Crystallogr.* **24,** 946–950.
PESKIN, C., ODELL, G. & OSTER, G. (1993). Cellular motions and thermal fluctuations: The Brownian ratchet. *Biophys. J.* **65,** 316–324.
PESKIN, C. & OSTER, G. (1995). Coordinated hydrolysis explains the mechanical behavior of kinesin. *Biophys. J.* **68,** 202–211.
RAY, S., MEYHOFER, E., MILLIGAN, R. & HOWARD, J. (1993). Kinesin follows the microtubule's protofilament axis. *J. Cell Biol.* **121,** 1083–1093.
RICE, S., LIN, A. W., SAFER, D., HART, C. L., NABER, N., CARRAGHER, B. O., CAIN, S. M., PECHATNIKOVA, E., WILSON-KUBALEK, E. W., WHITTAKER, M., PATE, E., COOKE, R., TAYLOR, E. W., MILLIGAN, R. A. & VALE, R. D. (1999). A structural change in the kinesin motor protein that drives motility. *Nature* **402,** 778–784.
SACK, S., MULLER, J., MARX, A., THORMAHLEN, M., MANDELKOV, E.-M., BRADY, S. T. & MANDELKOW, E. (1997). X-ray structure of motor and neck domains from rat brain kinesin. *Biochemistry* **36,** 16155–16165.
SCHNITZER, M. J., VISSCHER, K. & BLOCK, S. M. (1999). Force production by single kinesin motors. *Nature Cell Biol.* **2,** 718–723.
SVOBODA, K., SCHMIDT, C. F., SCHNAPP, B. J. & BLOCK, S. M. (1993). Direct observation of kinesin stepping by optical trapping interferometry. *Nature* **365,** 721–727.
SVOBODA, K. & BLOCK, S. M. (1994). Force and velocity measured for single kinesin molecules. *Cell* **77,** 773–784.
SVOBODA, K., MITRA, P. & BLOCK, S. (1994). Fluctuation analysis of motor protein movement and single enzyme kinetics. *Proc. Natl Acad. Sci. U.S.A.* **91,** 11782–11786.
VALE, R. D., FUNATSU, T., PIERCE, D. W., ROMBERG, L., HARADA, Y. & YANAGIDA, T. (1996). Direct observation of single kinesin molecules moving along microtubules. *Nature* **380,** 451–453.
VALE, R. D. & FLETTERICK, R. J. (1997). The design plan for kinesin motors. *Annu. Rev. Cell. Dev. Biol.* **13,** 745–777.
VAN KAMPEN, N. G. (1981). Stochastic process in physics and chemistry. Amsterdam: North-Holland Publ. Co.
VISSCHER, K., SCHNITZER, M. J. & BLOCK, S. M. (1999). Single kinesin molecules studied with a molecular force clamp. *Nature* **400,** 184–189.

APPENDIX A

Discussion of a possible effect of tether elasticity

Peskin & Oster (1995) assumed that the free head of the motor approaches thermal equilibrium much faster than the large, tethered bead. They demonstrated that, in this situation, the tether elasticity has a significant influence on the force–velocity relation. The difference in our model is that the free head does not move freely (restricted only by the length of the neck region), but rather transitions between the forward- and backward- pointing states. The order of magnitude of the delay time between such jumps can be estimated roughly as the diffusion time between the states, $\sim (10\ \mathrm{nm})^2/(10^7\ \mathrm{nm}^2/\mathrm{s}) \sim 10^{-5}\,\mathrm{s}$, multiplied by the Arrhenius factor, $\exp(5k_BT/k_BT) \sim 100$, where $5k_BT$ is the likely height of the energy barrier between the states. Thus, the characteristic time scale for the motion of the free head of kinesin is $10^{-3}\,\mathrm{s}$. A 0.5-μm bead diffusing against a 0.5 pN/nm spring equilibrates over $\sim (10^{-5}\,\mathrm{pN\,s/nm})/(1\ \mathrm{pN/nm}) \sim 10^{-5}\,\mathrm{s}$. (The characteristic time for a bead to equilibrate is its frictional coefficient, $\sim 10^{-5}\,\mathrm{pN\,s/nm}$, divided by the spring constant of the tether.) Therefore, the bead equilibrates almost instantly after the jump between the two states of the free head takes place. Then, until the next jump, we can assume that the average force, equal to the load force, is applied to the hinge between the heads. Based on this qualitative argument, we assume that the tether elasticity has only a small effect, and that the load force is applied directly to the hinge between the kinesin heads. In the future, if the effective potential energy of the neck region conformation is determined, we will then be able to examine more rigorously the effect of the tether elasticity.

APPENDIX B

Calculations of the dissociation rate, load–velocity relations and randomness parameter

Our analysis in the appendix follows closely the approach of Elston (2000). We will use the following notations:

$$\tilde{k}_2 = k_2 p(f), \quad \tilde{k}_3 = k_3(1 - p(f)),$$

$$\tilde{k}_4 = k_4(f) = k_4(0)\exp(-Lf/k_BT), \quad \text{(B.1)}$$

and

$$\rho(j, t) = \begin{pmatrix} z_j(t) \\ u_j(t) \\ s_j(t) \end{pmatrix}. \quad \text{(B.2)}$$

The Markov chain equations (3) can be rewritten in a matrix formulation:

$$\frac{\mathrm{d}\rho}{\mathrm{d}t} = \mathbf{A}\rho(j,t) + \mathbf{A}_+\rho(j-1,t), \qquad \text{(B.3)}$$

where

$$\mathbf{A} = \begin{pmatrix} -k_1 & 0 & 0 \\ k_1 & -(\tilde{k}_2+\tilde{k}_3) & 0 \\ 0 & \tilde{k}_3 & -\tilde{k}_4 \end{pmatrix},$$

$$\mathbf{A}_+ = \begin{pmatrix} 0 & \tilde{k}_2 & \tilde{k}_4 \\ 0 & 0 & 0 \\ 0 & 0 & 0 \end{pmatrix}. \qquad \text{(B.4)}$$

In order to find the average velocity, dissociation rate and displacement variance, we have to compute the moments of $j(t)$ (Van Kempen, 1987). A useful technique for calculating these moments is to consider the vector

$$\mathbf{R}(\zeta, t) = \sum_{j=-\infty}^{j=\infty} \zeta^j \rho(j,t).$$

It is straightforward to verify [also see Elston (2000)] that eqn (B.3) can be recast in the form:

$$\frac{\mathrm{d}\mathbf{R}}{\mathrm{d}t} = \mathbf{A}\mathbf{R} + \zeta\mathbf{A}_+\mathbf{R} = \mathbf{B}(\zeta)\mathbf{R},$$

$$\mathbf{B}(\zeta) = \begin{pmatrix} -k_1 & \zeta\tilde{k}_2 & \zeta\tilde{k}_4 \\ k_1 & -(\tilde{k}_2+\tilde{k}_3) & 0 \\ 0 & \tilde{k}_3 & -\tilde{k}_4 \end{pmatrix}. \qquad \text{(B.5)}$$

B.1. DISSOCIATION RATE

Components of the vector

$$\mathbf{R}(1,t) \equiv \begin{pmatrix} Z(t) \\ U(t) \\ S(t) \end{pmatrix} = \sum_{j=-\infty}^{j=\infty} \begin{pmatrix} z_j(t) \\ u_j(t) \\ s_j(t) \end{pmatrix}$$

designate the probability of the motor being in the zippered, unzippered and strained states, respectively. Based on these designations, the following equality holds:

$$Z(t) + U(t) + S(t) = 1. \qquad \text{(B.6)}$$

Steady-state solutions of system (B.5) at $\zeta = 1$ are restricted by condition (B.6) and are given by the following formulae:

$$U = \left[1 + \frac{\tilde{k}_2+\tilde{k}_3}{k_1} + \frac{\tilde{k}_3}{\tilde{k}_4}\right]^{-1},$$

$$S = \frac{\tilde{k}_3}{\tilde{k}_4}\left[1 + \frac{\tilde{k}_2+\tilde{k}_3}{k_1} + \frac{\tilde{k}_3}{\tilde{k}_4}\right]^{-1},$$

$$Z = \frac{\tilde{k}_2+\tilde{k}_3}{k_1}\left[1 + \frac{\tilde{k}_2+\tilde{k}_3}{k_1} + \frac{\tilde{k}_3}{\tilde{k}_4}\right]^{-1}. \qquad \text{(B.7)}$$

The dissociation rate γ can be computed as the dissociation rate from the unzippered state, k_u, factored by the probability of this state, U, plus the dissociation rate from the strained state, k_s, factored by the probability of this state, S:

$$\gamma = k_u U + k_s S. \qquad \text{(B.8)}$$

Substituting expression (B.7) into eqn (B.8), we obtain formula (5).

B.2. LOAD DEPENDENCE OF VELOCITY AND RANDOMNESS PARAMETER:

Let $\lambda_0(\zeta)$ denote the largest eigenvalue of matrix $\mathbf{B}(\zeta)$. It is easy to see in the special case of $\zeta = 1$, that the largest eigenvalue of transition matrix $\mathbf{B}(1)$ is equal to 0: $\lambda_0(1) = 0$. Elston (2000) demonstrated that:

$$\langle j\rangle = \lambda_0'(1)t + O(1), \quad \langle j^2\rangle - \langle j\rangle^2 = (\lambda_0''(1) + \lambda_0'(1))t + O(1), \qquad \text{(B.9)}$$

where $\lambda_0'(\zeta) = \mathrm{d}\lambda_0(\zeta)/\mathrm{d}\zeta$, and $\lambda_0''(\zeta) = \mathrm{d}^2\lambda_0(\zeta)/\mathrm{d}\zeta^2$. These formulae are very useful, because they allow us to express the average velocity, $\langle u\rangle$, and the effective diffusion coefficient of the motor, D

$$\langle v\rangle = \delta \lim_{t\to\infty} \frac{\langle j\rangle}{t}, \quad D = \delta^2 \lim_{t\to\infty} \frac{\langle j^2\rangle - \langle j\rangle^2}{2t},$$

in terms of the first two derivatives of the largest eigenvalue of matrix $\mathbf{B}(\zeta)$:

$$\langle v\rangle = \delta\lambda_0'(1), \quad D = \frac{\delta^2}{2}(\lambda_0''(1) + \lambda_0'(1)).$$

The randomness parameter, r, is defined as (Svoboda *et al.*, 1994)

$$r = \frac{2D}{\delta \langle v \rangle} \ . \tag{B.10}$$

To find the derivatives of the largest eigenvalue of matrix $\mathbf{B}(\zeta)$, let us consider the characteristic equation

$$\det[\mathbf{B}\mathbf{G}(\zeta) - \lambda \mathbf{I}] = 0.$$

This equation has the following form:

$$\begin{aligned} &\lambda^3 + (k_1 + \tilde{k}_2 + \tilde{k}_3 + \tilde{k}_4)\lambda^2 + (k_1\tilde{k}_4 \\ &\quad + (k_1 + \tilde{k}_4)(\tilde{k}_2 + \tilde{k}_3) - k_1\tilde{k}_2\zeta)\lambda \\ &\quad + k_1\tilde{k}_4(\tilde{k}_2 + \tilde{k}_3)(1 - \zeta) = 0. \end{aligned} \tag{B.11}$$

Let us introduce a small variable $\alpha \ll 1$, such that $\zeta = 1 + \alpha$. We can use a Taylor series expansion of $\lambda_0(\zeta)$:

$$\lambda_0(1 + \alpha) = \alpha\lambda_0'(1) + \frac{\alpha^2}{2}\lambda_0''(1) + \cdots$$

Substituting this expansion and expression $\zeta = 1 + \alpha$ into the characteristic eqn (B.11) and setting the coefficients in front of α and α^2 equal to zero, we find the first two derivatives of $\lambda_0(\zeta)$ at $\zeta = 1$:

$$\lambda_0'(1) = \frac{K_3}{K_2 - k_1\tilde{k}_2}, \ \lambda_0''(1) = 2\lambda_0'(1)\frac{k_1\tilde{k}_2 - K_1\lambda_0'(1)}{K_2 - k_1\tilde{k}_2}, \tag{B.12}$$

where

$$\begin{aligned} K_1 &= k_1 + \tilde{k}_2 + \tilde{k}_3 + \tilde{k}_4, \\ K_2 &= k_1\tilde{k}_4 + (k_1 + \tilde{k}_4)\,(\tilde{k}_2 + \tilde{k}_3), \\ K_3 &= k_1\tilde{k}_4(\tilde{k}_2 + \tilde{k}_3). \end{aligned} \tag{B.13}$$

Using eqns (B.12) and (B.13), we obtain the formulae for the average velocity and the randomness parameter:

$$\begin{aligned} \langle v \rangle &= \delta \frac{K_3}{K_2 - k_1\tilde{k}_2}, \\ r &= 1 + 2\frac{k_1\tilde{k}_2(K_2 - k_1\tilde{k}_2) - K_1K_3}{(K_2 - k_1\tilde{k}_2)^2}, \end{aligned} \tag{B.14}$$

which result in eqns (4) and (6), respectively.